

Application of Continuum Models to Deformation of the Aleutian Island Arc

ERIC L. GEIST AND DAVID W. SCHOLL

U. S. Geological Survey, Menlo Park, California

Continuum models were constructed to describe large-scale deformation of the Aleutian Island Arc over the past 5 m.y. These models consider the island arc as a continuum in the horizontal plane with the velocity boundary condition at the Pacific edge stated as a fraction of Pacific plate convergence transferred to the arc. First, a simple model of uniformly distributed strain is formulated to illustrate the mechanics of continuous deformation. Lineaments along the arc massif rotated about a vertical axis are matched by small-element rotation calculated from the model. However, this model does not predict across-arc variations in deformation and produces an unrealistic amount of crustal thickening after 5 m.y. A physically more meaningful model of deformation is the thin viscous sheet model based on averages of stress and rheology throughout the lithosphere. The amount of motion transferred from the Pacific plate to the arc is constrained by the rotated lineaments, while the effective stress-strain exponent (n) and the ability the lithosphere has to sustain crustal thickness contrasts (the Argand number) are independent variables. Primarily, bathymetry, earthquake focal mechanisms, and styles of faulting are used to evaluate the models. The preferred model is one where the amount of motion transferred from the Pacific plate is greater in an arc-parallel direction than in an arc-normal direction, producing stresses consistent with strike-slip faulting at the far western end of the arc and tensional stresses consistent with transverse normal faulting elsewhere in the arc massif. This model agrees with observations of slip vectors by Ekström and Engdahl (1989), who conclude that a portion of the arc-parallel component of relative plate motion is taken up in the overriding plate. This model implies that compressive stress transferred to the arc is small in comparison to along-arc shear stress and that stresses conducive to strike-slip faulting are prevalent throughout the arc.

1. INTRODUCTION

Over the past 5 m.y., the massif of the Aleutian Island Arc has been complexly deformed by strike-slip faulting, normal faulting, and block rotation. Numerous lineaments thought to represent faults and fractures are observed in the bathymetry and in radar images of the islands [Vallier *et al.*, 1991]. These lineaments exhibit a wide range of orientation and, where offset can be deduced from seismic reflection data, have an equally wide ranging sense of movement. This distributed deformation across the width of the arc leads us to model the deformation as a continuous medium. Although individual faults are not described by a continuous medium, results from these models represent deformation averaged over tens and hundreds of kilometers and can be correlated to broad regions of the arc where the style of deformation is similar. The critical factor controlling deformation is the average of the mechanical properties over the thickness of the lithosphere. Viscous fluid flow of the lower lithosphere is assumed to control the deformation, although the mechanical properties of the brittle upper crust are included and can even dominate the average mechanical properties of the lithosphere.

Similar models have been developed and successfully used to describe deformation at continental collision zones [Tapponnier and Molnar, 1976; England and McKenzie, 1982; England and Houseman, 1986], along strike-slip zones [Bird and Piper, 1980; Bird and Baumgardner, 1984; Sonder *et al.*, 1986], in areas of continental extension [England, 1983; Sonder and England, 1989], and for the Laramide orogeny in the western United States [Bird, 1989]. The length scale of the observations in these models is typically of the order of several hundred to thousands of kilometers. It has yet to be demonstrated that such models can be applied to narrow zones of deformation zones a few hundred kilometers wide that span island arcs.

This paper is not subject to U.S. copyright. Published in 1992 by the American Geophysical Union.

Paper number 91JB02992.

Previous models of island arc deformation have considered the elastic, plastic, and viscoelastic response of the oceanic plate to subduction [e.g., Davies, 1981; Tharp, 1985; Sato and Matsu'ura, 1988], stresses induced by viscous flow in the lower lithosphere of the subducted plate [Melosh and Raefsky, 1980; Zhang *et al.*, 1985], and stresses induced by density variations and asthenospheric flow [Sleep, 1975]. These models predict, with varying degrees of success, bathymetric and gravity observations across the arc. However, these models have not analyzed along-arc variations in deformation that arise from lateral changes in the boundary conditions. Three-dimensional finite element models using viscoelastic and linearly viscous rheologies have been developed by Hashimoto [1984, 1985] and subsequently applied by Yoshioka and Hashimoto [1989], Yoshioka *et al.* [1989], Ghose *et al.* [1990], and Yoshioka [1991]. They have been successful in using these models to describe stress accumulation and interplate coupling. The objective of this study is to determine whether continuum models in the horizontal plane can describe deformation of island arcs, and to observe the response of arc deformation to nonlinear rheologies and changes in mechanical properties of the arc. Here the emphasis is on map view deformation of the arc caused by the laterally varying horizontal forces from oceanic plate convergence, rather than on deformation caused by vertical forces associated with the bending of the subducted plate. The observations used to evaluate the models are from the arc massif. It should be recognized that in the trench and outer forearc regions, the vertical forces associated with subduction are likely to have more of an effect on deformation than the horizontally transmitted forces from convergence which are manifested most strongly toward the crestal region of the arc massif.

2. TECTONIC HISTORY OF THE ALEUTIAN ISLAND ARC

Scholl *et al.* [1987] describe the evolution of the Aleutian Island Arc as occurring in three phases: initial phase (55?-42 Ma), medial phase (42-5 Ma), and modern phase (5 Ma to present). Each of these phases correspond to approximately dated rock

series, lower, middle and upper, described by *Marlow et al.* [1973], *Scholl et al.* [1987], and *Vallier et al.* [1991].

The formation of the arc resulted from a southward jump of the subduction zone from the Beringian-Siberian margin of the north Pacific to its present offshore location. A piece of the Kula plate, termed the Aleutia terrane by *Marlow and Cooper* [1983], was accreted to the North American plate forming the basement of the Aleutian Basin and possibly that of the Aleutian Island Arc [*Cooper et al.*, 1976; *Kay and Kay*, 1985]. Rapid magmatic growth of the arc began to wane in late middle Eocene time, commencing with a shift of the Pacific Euler pole at 43 Ma that caused more oblique convergence along the arc [*Duncan and Clague*, 1985; *Engebretson et al.*, 1986].

The medial phase was characterized by decreased igneous activity and elevation of the arc crest. Although constructional magmatism slowed, plutonism along the arc crest was prevalent. Sustained uplift of the arc crest is thought to be linked to the subduction of increasingly younger oceanic crust generated at the Kula-Pacific spreading ridge and the emplacement of middle series calc-alkaline epizonal plutons. Although flank magmatism was greatly suppressed, thick blankets of volcanoclastic debris accumulated on the slope of the Aleutian Island Arc.

The past 3-5 m.y. of the arc's history has been a time of accelerated deformation, including regional subsidence of the arc summit, subduction of the extinct (as of 43 Ma) Kula-Pacific Ridge, compressional deformation of the outer forearc, and the rapid formation of intra-arc summit basins in conjunction with shearing of the arc massif. Convergence of the Pacific plate with the arc shifted to a more orthogonal direction in response to a Pacific Euler pole shift at 3-5 Ma [*Engebretson et al.*, 1986]. This shift initiated the latest phase of volcanism along the arc. Compressional deformation along the outer forearc occurred in conjunction with, and was perhaps related to, formation of a thick subduction complex. This complex is thought to have accumulated in response to flooding of the trench axis with sediment derived from the glaciated drainages of the Gulf of Alaska [*McCarthy et al.*, 1984; *McCarthy and Scholl*, 1985]. Thickening of the subduction complex and right-lateral shearing in the outer forearc formed structural highs that trapped large amounts of late Tertiary and younger sediment in forearc basins [*Harbert et al.*, 1986; *Ryan and Scholl*, 1989].

Also in the modern phase, the arc massif was fragmented by left-lateral faults transverse to its trend and manifested by high-relief Pacific slope canyons (described by *Gibson and Nichols* [1953], *Gates and Gibson* [1956], *Perry and Nichols* [1965], *Anderson* [1971], *LaForge and Engdahl* [1979], and *Spence* [1977]). As noted by *Geist et al.* [1988], the "blocks" between faults delimit domains of similar deformation styles, rather than rigid and coherent rocks (Figure 1). Under oblique convergence, rocks within the block boundaries have rotated clockwise, forming extensional summit basins in their wake [*Geist et al.*, 1988]. Rotation along the arc is measured from the following lineaments: the scarp bounding Ingenstrem depression along its southwest side (IDST), the scarp bounding Pennant basin along its northeast side (PBST), the Amchitka Island trend (AKIT), the Delarof Island trend (DIT), and the Amliia Island trend (AMIT). West of 175° E, the dominant mode of deformation changes from block rotation to strike-slip faulting generally parallel with the trend of the arc. In summary, the different styles of deformation in the modern phase of the arc include (1) right-lateral strike-slip and thrust faulting near the Pacific edge [*Ryan and Scholl*, 1989], (2) left-lateral transtensional faulting on transverse faults, (3) right-lateral strike-

slip and normal faulting on arc-parallel faults near the North American edge, and (4) dominant right lateral strike-slip faulting in the western part of the arc. The kinematic analysis of *Geist et al.* [1988] links the observed structures to a model of discrete blocks surrounded by shear zones but does not address the origin of these structures in relation to tectonic forces, as is attempted in this study.

3. GEOMETRY AND BOUNDARY CONDITIONS

The continuum models described below are developed using cylindrical coordinates so that the boundaries of the deforming zone are at $r_0=1950$ km and $r_1=2170$ km and the $\theta=0$ line is coincident with the point where the Pacific plate motion vector is parallel with the arc (Figure 2a).

Velocity boundary conditions are used for the inner and outer arcs of the deforming zone, while no prescribed boundary conditions are given for the ends of the arc. Boundary conditions can also be stated in terms of stress, as *Sonder et al.* [1986] have done, although more is known about the boundary velocities than the boundary stresses. *Wdowski and O'Connell* [1990] make the distinction that time-invariant stress boundary conditions imply a constant tectonic force applied at the boundary, while time-invariant velocity boundary conditions imply a constant net force that includes both tectonic and buoyancy forces. For island arcs, the buoyancy forces may be significant, but as demonstrated later, they are not likely to change appreciably as deformation progresses.

The boundary conditions at the active boundary (subduction zone) should take into account the body and surface forces acting on the arc including slab pull, ridge push, asthenospheric flow, and crustal buoyancy of the island arc crust [*Sleep*, 1975; *Hashimoto*, 1985]. Rather than estimating each of these forces and in order to cast the model in two dimensions, we initially assume that these forces result in velocity vectors oriented parallel to those of Pacific plate motion. The magnitude of the velocity vectors at the active boundary must be a fraction of Pacific plate motion to allow for subduction (i.e., perfect coupling cannot exist). The velocity of the Pacific plate at the Pacific edge of the arc is defined by the Euler pole rotation of *Engebretson et al.* [1986] (Figure 1) and is approximated by the following sinusoids:

$$u(r_1, \theta) = \alpha_r u_0 \sin(\beta_r \theta) \quad v(r_1, \theta) = \alpha_\theta v_0 \cos(\beta_\theta \theta), \quad (1)$$

where u and v are the radial and tangential components of the velocity vector, respectively (i.e., $\mathbf{u} = (u, v, w)$), and u_0 , v_0 , β_r , and β_θ are constants given in Table 1. The variables α_r and α_θ represent the fraction of Pacific plate velocity that is transferred to the overriding plate. Velocity boundary conditions stated as a fraction of the converging plate velocity are similarly used to explain slip vectors in the main thrust zone of the Aleutian Island Arc by *Ekström and Engdahl* [1989]. At the inner or North American boundary, the horizontal velocity components equal zero and are continuous from the deformation zone (Figure 2b). This is consistent with the lack of significant folding or faulting observed in the Aleutian Basin section north of the Aleutian Island Arc [*Scholl et al.*, 1987].

In our models, the boundary conditions do not vary with depth, indicating that the traction acting on the Pacific edge can be related to a normal stress component (σ_{rr}) and a shear stress component ($\sigma_{r\theta}$). In actuality, the traction applied to the arc acts on a dipping boundary coincident with the main thrust zone [*Bird*,

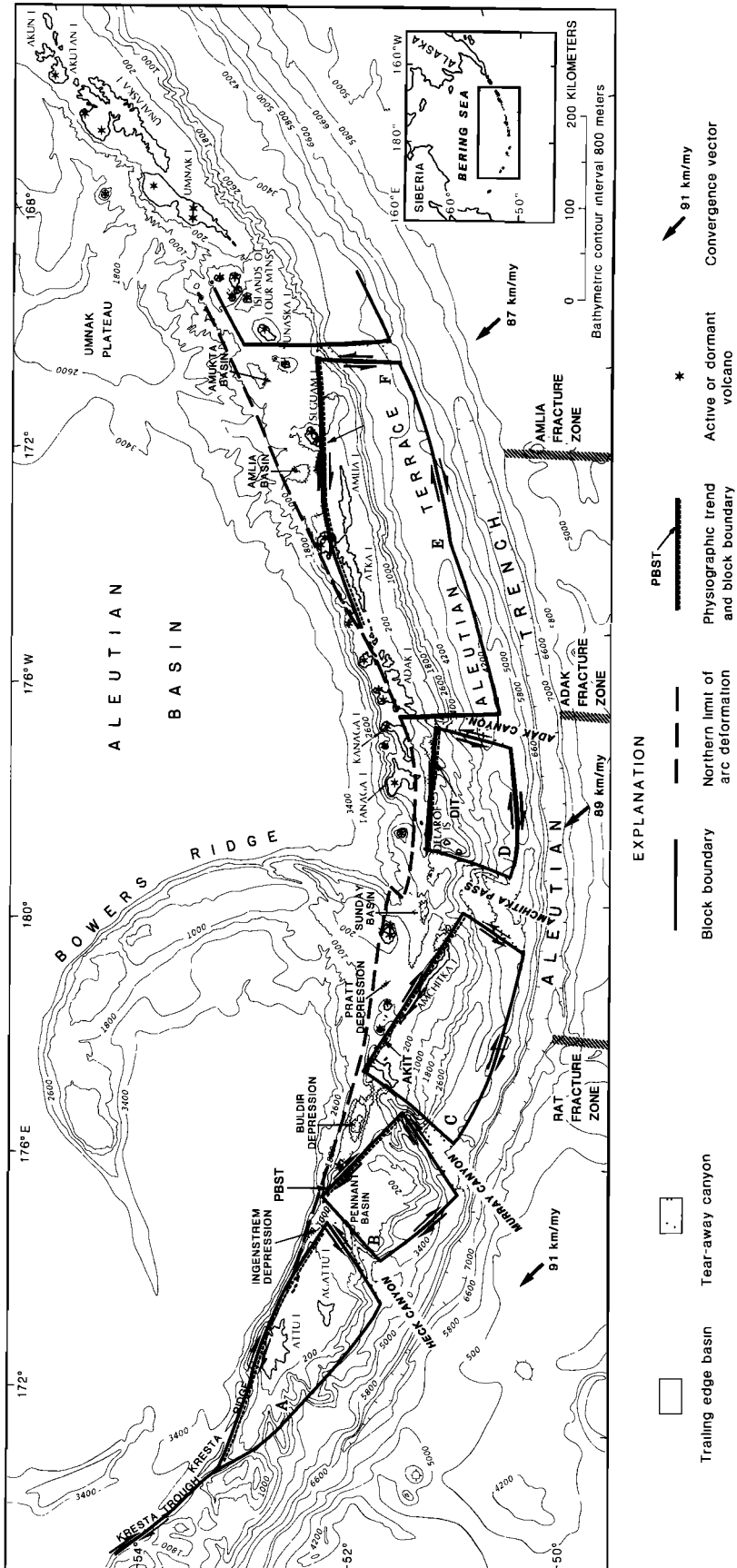


Fig. 1. Regional bathymetric map (contour interval of 800 m) of Aleutian Island Arc showing major islands and tectonic blocks (modified from Geist *et al.* [1988]). The blocks are designated as follows: A, Near block; B, Buldir block; C, Rat block; D, Delarof block; E, eastern Andreanof block; and F, western Andreanof Block. Rotated lineaments include IDST, scarp along southwest side of Ingenstrom Depression; PBST, scarp along northeast side of Pennant basin; AKIT, Amchitka Island trend; DIT, Delarof Island trend; AMIT, Amliia Island trend.

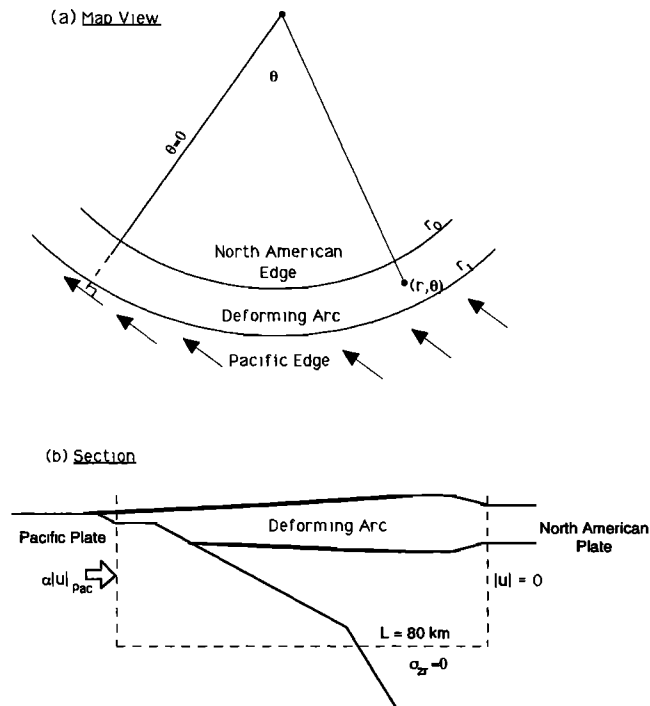


Fig. 2. Diagram of model geometry. (a) Model in map view showing variation of boundary velocity vectors. (b) Model in cross section showing single depth-averaged value for each of the boundary conditions. Dashed lines show boundaries of deforming arc in model. L is the thickness of the lithosphere.

TABLE 1. Parameters Used in Models

Description		Values
Ar	Argand number	$1, 3^*, 30^*, 10^2, 10^3, 10^4$
g	gravitational acceleration	9.8 m s^{-2}
L	lithospheric thickness	80 km
n	effective stress-strain exponent	1, 3, 10, 1000
r_0, r_1	inner and outer radii of arc	1950 km, 2170 km
s_0	initial crustal thickness	17 km
u_0, v_0	velocity coefficients	83, 95 km my $^{-1}$
α_θ	fraction of Pacific plate motion in arc-parallel direction	0.09-0.40 †
α_r	fraction of Pacific plate motion in arc-normal direction	0.05-0.40 †
β_r, β_θ	spatial "wavelength" for boundary conditions	1.32, 1.32
ρ_c	density of crust	2.95 Mg m^{-3}
ρ_m	density of mantle	3.30 Mg m^{-3}

*Not shown.

† Constrained by rotated lineaments.

1978] and can be related to a normal stress component across the boundary and two shear stress components: one parallel to the arc and one in the downdip direction. A model formulated in the horizontal plane becomes less accurate with decreasing dip of the main thrust zone owing to the increasing effect of the downdip shear traction down to the brittle-ductile transition. In addition, the assumption of constant crustal thickness does not hold in the forearc where the crust tapers toward the trench. Thus the model probably is least accurate in the forearc region. However, farther away from the active margin, it is difficult to gauge the effect of

assuming a two-dimensional traction applied at the trench. Qualitatively, one can note that the stress magnitudes produced by the thin viscous sheet model (described later) are comparable to the stress magnitudes estimated by *Froidevaux et al.* [1988] for arcs worldwide, thus indicating that the models are not predicting unrealistic stress regimes. Furthermore, the three-dimensional models using a linearly viscous rheology developed by *Hashimoto* [1985] show that while the principal stress orientation and magnitude can vary substantially across the forearc, they tend to be constant farther away from the trench (as is generally observed for the thin viscous sheet models described in this paper).

4. MODEL I: UNIFORMLY DISTRIBUTED STRAIN

In an attempt to explain the rotation of lineaments along the Aleutian Island Arc, we first consider the simple model where strain is uniformly distributed across the arc. This model was introduced by *McKenzie and Jackson* [1983], and although it does not invoke a particular material model, it is an important foundation for interpreting more complex models and understanding the basic mechanics of continuous deformation (see also *Cox* [1980]). This model is defined as having constant velocity gradients everywhere in the deforming region with the boundary conditions specified in section 3.

The velocity vector field shown in Figure 3a is derived from the previous boundary conditions with the constraint of a constant velocity gradient (i.e., $\partial \mathbf{u} / \partial r = \text{const}$). The vertical axis rotation calculated from the velocity field can be compared with rotated lineaments along the length of the arc. *McKenzie and Jackson* [1983] point out two distinct types of rotation: (1) small rigid body rotation within the deforming fluid and (2) rotation of material vectors as part of the fluid. We assume that rotation measurements from block rotation fall into the first category since the lineaments used for those measurements are small relative to the scale of the deforming zone. Furthermore, if the rigid elements are equidimensional, the instantaneous rate of rotation is given as half of the vertical component of vorticity or

$$\frac{\partial \psi}{\partial r} = \frac{1}{2}(\nabla \times \mathbf{u}) \quad (2)$$

where ψ is the amount of rotation. The total amount of rotation the lineaments have undergone in the modern phase is equation (2) integrated over 5 m.y. Figure 4 shows the regional trend of finite rotation defined by lineaments within the arc mass and the rotation calculated from the model along the North American edge (where the rotated lineaments are located). Two broad regions of unrotated rocks exist (Figure 1): block A (Near block), predominantly deformed by throughgoing strike-slip faults [*Geist et al.*, 1988], and block E, possibly pinned from rotation by medial phase plutonic bodies (H. F. Ryan and D. W. Scholl, manuscript in preparation, 1992). A boundary condition of 46% of the Pacific plate velocity produces good agreement with measurements of rotated lineaments (Figure 4). Figure 3b shows that the small-element rotation after 5 m.y. is almost constant across the width of the arc. It should be noted that information on the arc-normal variation of small-element rotation is lacking and that such variation may not conform with the constant velocity gradient model as was shown by *England and Wells* [1991] for Oregon and Washington.

The rate of crustal thickening can be derived analytically [*McKenzie and Jackson*, 1983] assuming incompressibility ($\nabla \cdot \mathbf{u} = 0$) and a constant initial crustal thickness (17 km from estimates

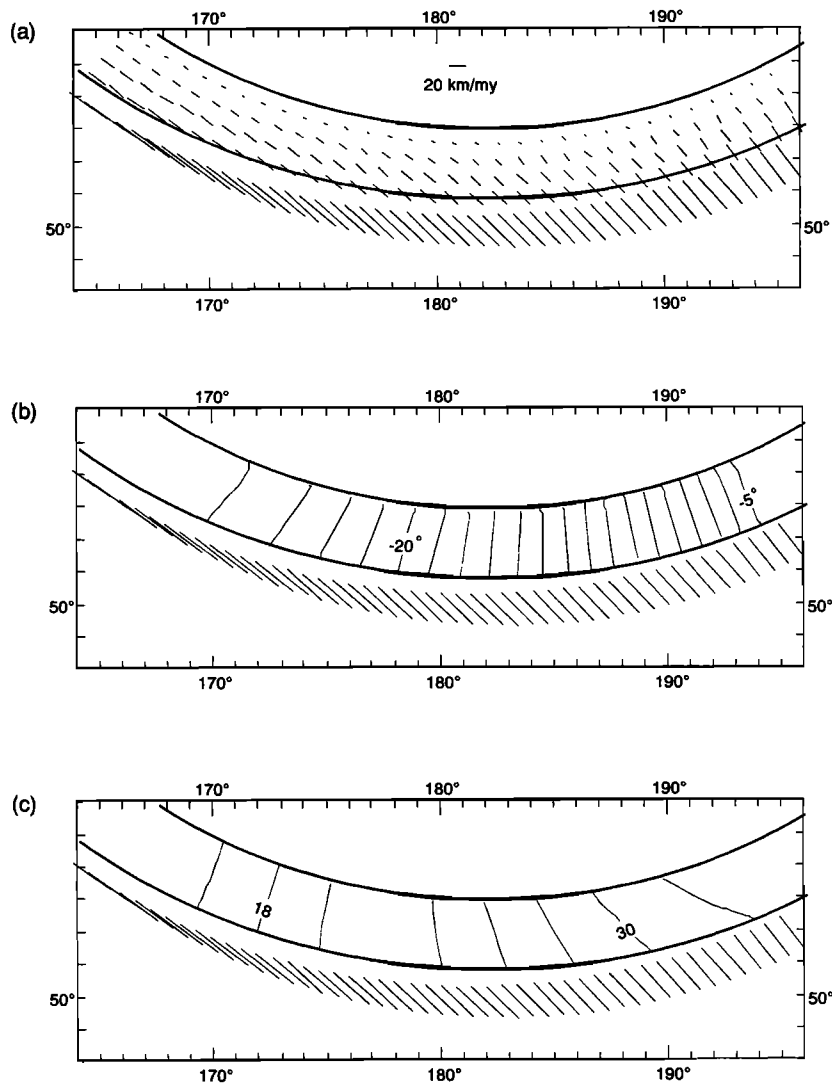


Fig. 3. Results from the constant velocity gradient model: (a) resulting velocity field, (b) net rotation after 5 m.y. calculated from the velocity field (contour interval is 1°), and (c) net crustal thickness calculated from the velocity field assuming 17 km initial thickness (contour interval is 2 km). 46% of the Pacific plate velocity was used as a boundary condition to to match the rotation of lineaments (Figure 4). Pacific plate velocity vectors are shown south of the Pacific edge of the arc.

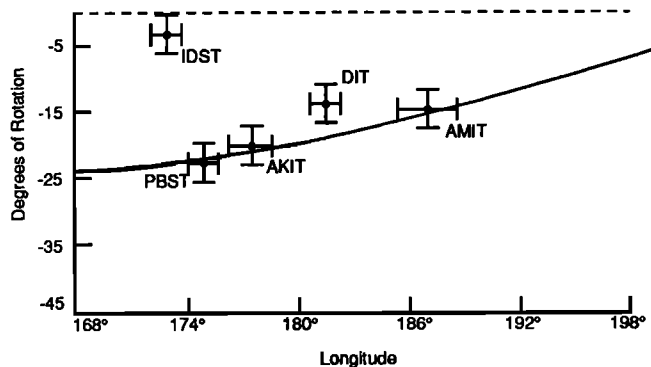


Fig. 4. Comparison of net rotation after 5 m.y. for the constant velocity gradient model (solid line) to rotated lineaments along the arc (Figure 1). 46% of the Pacific plate motion transferred to the arc is used to produce this best fit curve (i.e., $\alpha_r = \alpha_\theta = 0.46$). Error bars on rotated lineaments indicate the approximate length of physiographic feature and uncertainty of rotation measured from bathymetric maps. See Figure 1 for abbreviations of lineament names.

made by *Shor* [1964], *Gaynanov et al.* [1968], and *Grow* [1973]). Using 46% of the Pacific plate velocity as a boundary condition, the amount of crustal thickening after 5 m.y. is shown in Figure 3c. Note here also that the predicted crustal thickness does not vary significantly across the arc, except at the eastern end. Although crustal thickness along the Aleutian Island Arc is significantly affected by the intrusion of subduction related magmas [*Kay and Kay*, 1985], a 30-35 km thick crust predicted for the eastern part of the arc is unrealistic. Also, the large arc-parallel gradient in crustal thickness predicted by this model does not agree with the constant width and elevation of the summit platform (an erosional surface).

The constant velocity gradient model illustrates that a simple continuum model that does not take into account physical properties can predict the rotation of lineaments along the Aleutian Island Arc. However, other quantities such as crustal thickness or across-arc variations in deformation that presumably arise from viscous and plastic behavior of the arc illustrate the need for more complex models.

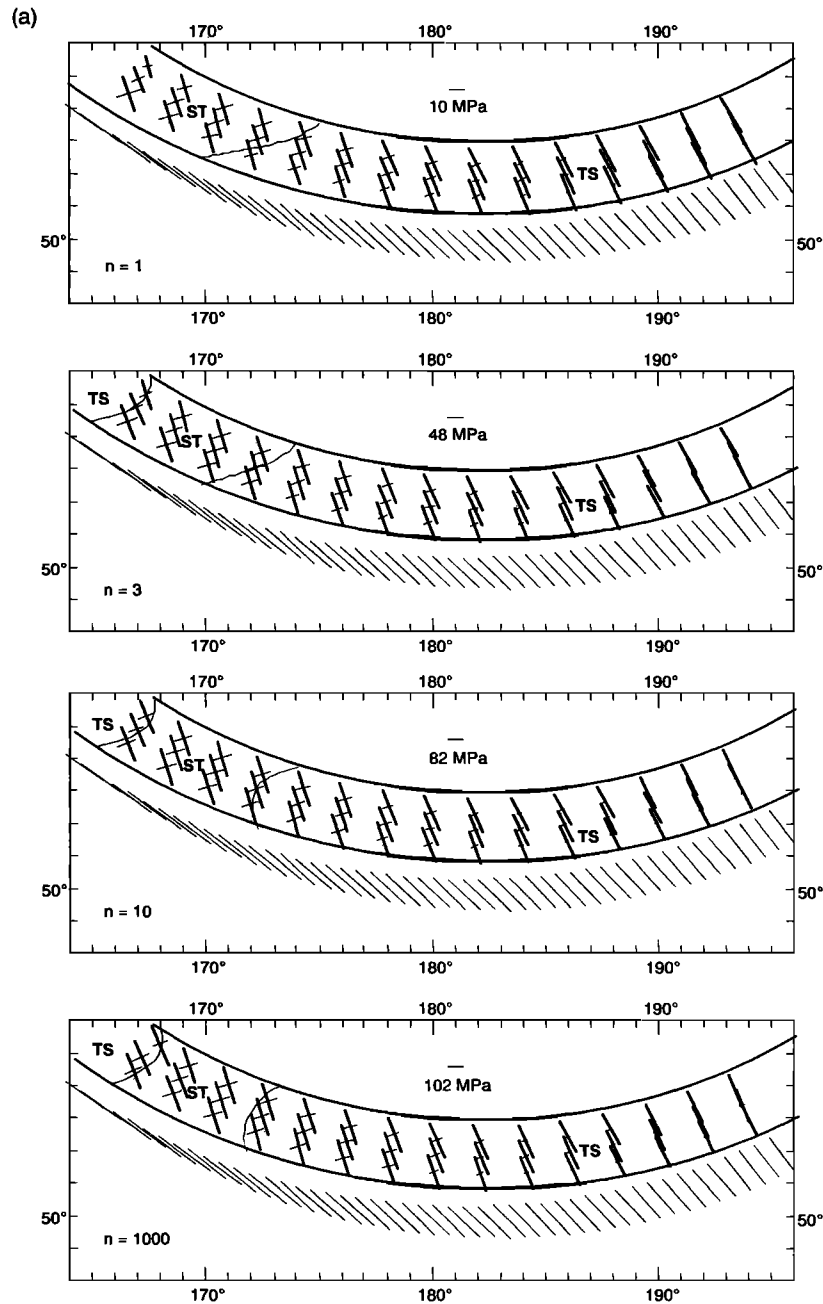


Fig. 5. (a) Principal horizontal deviatoric stresses and (b) crustal thickness for the thin viscous sheet model after 5 m.y. for $n=1, 3, 10,$ and 1000 . For this and following figures, relative scale for stresses (in megapascals) is shown for each model with thicker line indicating compressive stress. Thin solid line in Figure 5a separates regions of similar faulting styles [Houseman and England, 1986]. ST, strike-slip with secondary thrust faulting; TS, thrust with secondary strike-slip faulting; etc. Initial crustal thickness and crustal thickness at Pacific and North American edges throughout time are 17 km. The Pacific edge boundary condition was chosen to produce the best fit to the rotated lineaments as in Figure 4 and is $\alpha_r = \alpha_\theta = 0.30$ for all values of n . $Ar=1$ for each case. Contour interval for crustal thickness diagrams is 2 km. Pacific plate velocity vectors are shown south of the Pacific edge of the arc.

5. MODEL II: THIN VISCIOUS SHEET

Description of model

The thin viscous sheet model developed by England and McKenzie [1982, 1983] and described in Appendix A is a more physically meaningful model than the previous model in that the equations of motion and a power law rheology are used to describe the deforming arc. The primary physical properties incorporated in the thin viscous sheet equation are the ability of the crust to sustain thickness contrasts (the Argand number) and

the effective stress-strain exponent (n). Several assumptions made in the thin viscous sheet model are common to all continuum models: strain must be continuously distributed in the zone of deformation, or as an approximation, only small amounts of slip can occur on many faults distributed throughout the zone. Rigid blocks in the brittle layer cannot interfere with the flow, such that these blocks ride passively on the ductile substrate. The strength of the brittle layer, however, can be explicitly accounted for since the rheology is averaged over the whole lithosphere, including the upper crust.

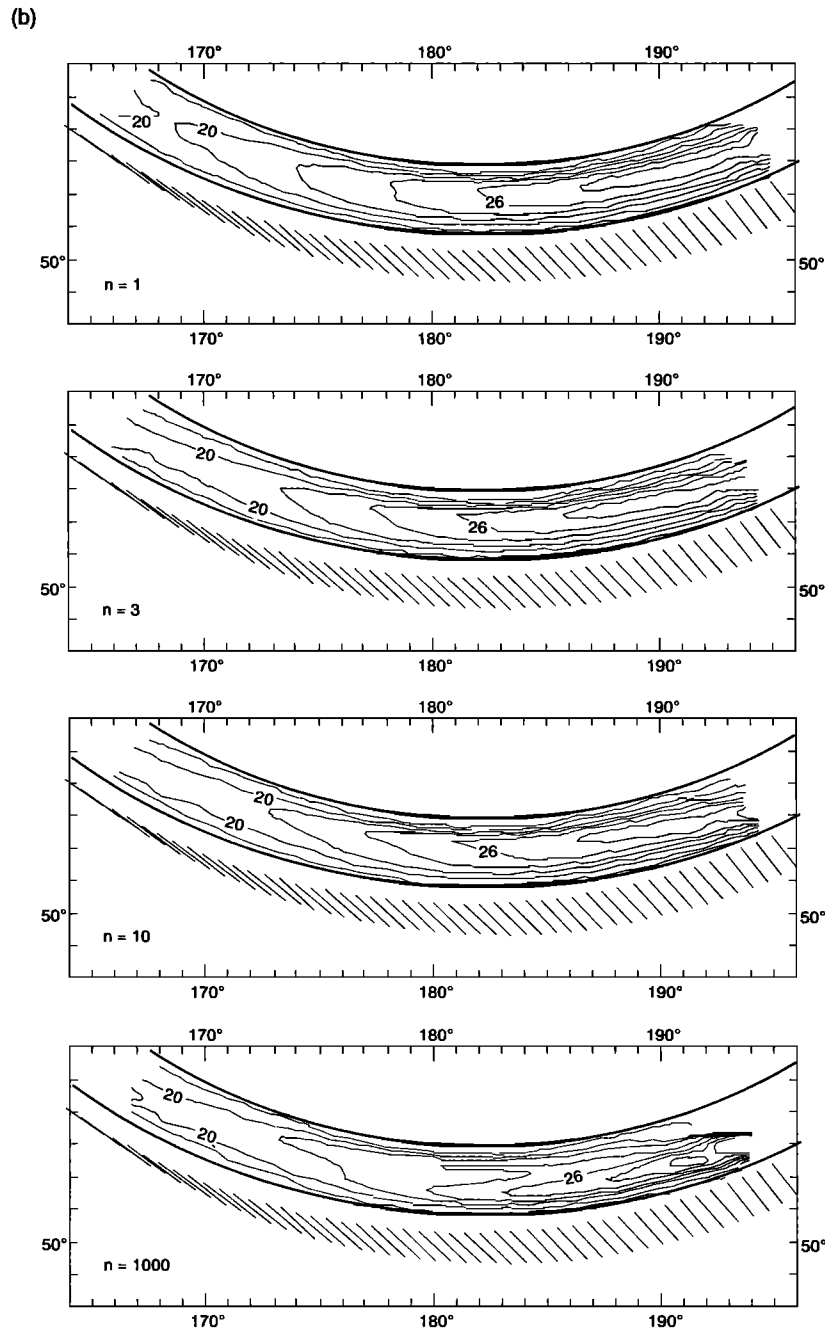


Fig. 5. (continued)

The thin sheet assumption maintains that no shear traction occurs at the base or top of the lithosphere and that no vertical variations exist in the horizontal velocity or stress components; or equivalently, that the width of the deforming zone is small compared to the thickness of the lithosphere. Because the width of island arcs is smaller than the width of continental deformation zones, it is important to test this assumption as it applies to arcs only several hundred kilometers wide. The width-to-thickness ratio for the Aleutian Island Arc is approximately 3:1, which is at the accuracy limit stated by *Artyushkov* [1973] for the thin sheet assumption. A quantitative discussion of the accuracy of the thin sheet assumption is given in Appendix B.

The Argand number (Ar) is defined by *England and McKenzie* [1982] as

$$Ar = \frac{g\rho_c(1-\rho_c/\rho_m)L^{(1+1/n)}}{Bu_0^{1/n}} \quad (3)$$

where ρ_c and ρ_m are the crust and mantle densities, respectively; L is the lithospheric thickness; u_0 is the characteristic velocity; and B is a constant that includes the temperature dependence of rheology averaged throughout the lithosphere. The Argand number is a measure of stress derived from the difference in crustal thickness divided by the average stress needed to produce the characteristic strain rate u_0/L . Equivalently, the Argand number is inversely related to the vertically integrated strength of the lithosphere as explained by *Sonder and England* [1986]. An Argand number of 0 implies that large contrasts in crustal

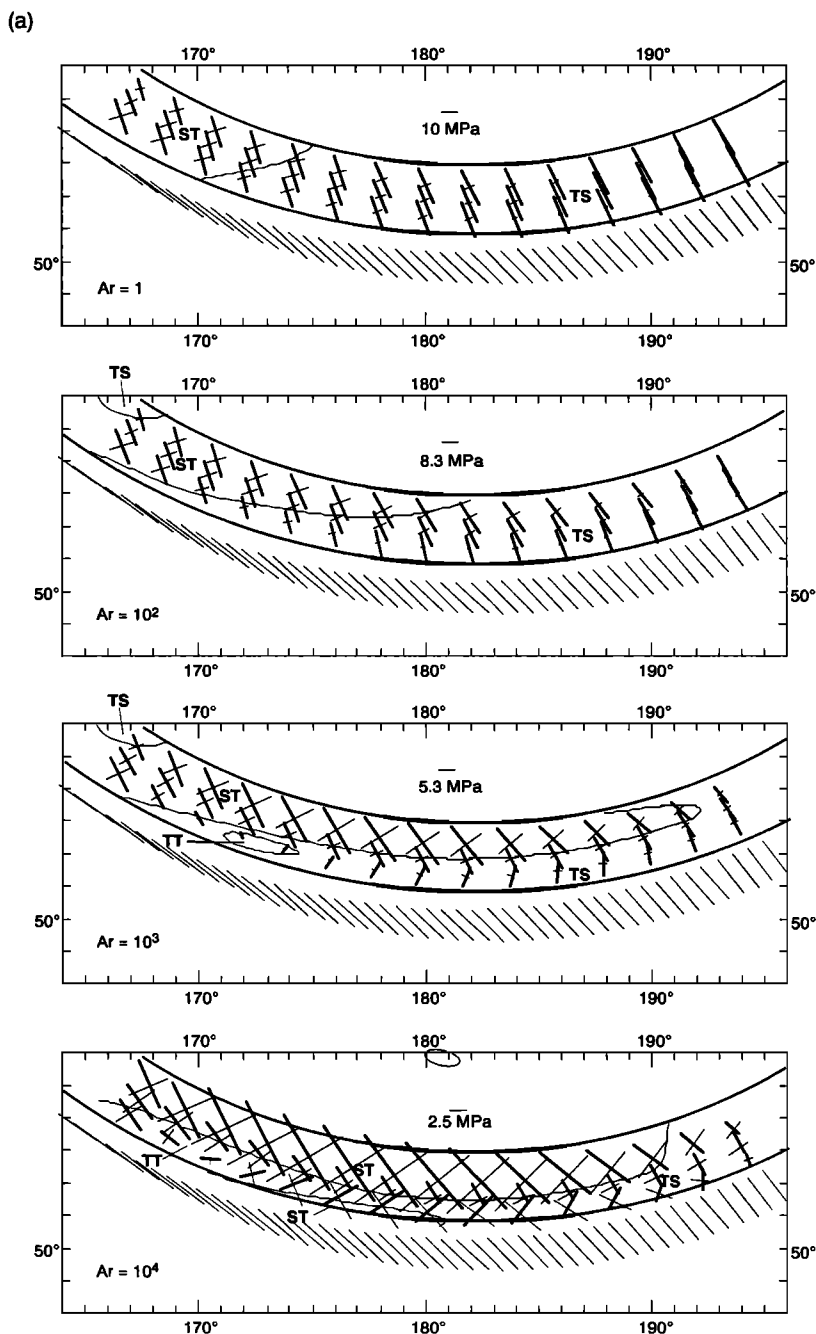


Fig. 6. (a) Principal horizontal deviatoric stresses and (b) crustal thickness for the thin viscous sheet model after 5 m.y. for $Ar=1, 10^2, 10^3, 10^4$. Thin solid line in Figure 6a delineates regions of similar faulting styles [Houseman and England, 1986]. The Pacific edge boundary condition was chosen to produce the best fit to the rotated lineaments as in Figure 4. For $Ar=1, 10^2, 10^3, 10^4$, $\alpha_r = \alpha_\theta = 0.30, 0.25, 0.17, 0.09$, respectively. $n=1$ for each case. Contour interval for crustal thickness diagrams is 2 km for $Ar = 1, 10^2$ and 1 km for $Ar = 10^3, 10^4$. Pacific plate velocity vectors are shown south of the Pacific edge of the arc.

thickness can be achieved, whereas a very large Argand number implies plane horizontal strain [Sonder *et al.*, 1986].

The rheology of lithosphere underlying island arcs as a function of depth is poorly understood. For a particular tectonic setting, the rheology of the lithosphere depends on the geothermal gradient, crustal thickness, and crustal composition [Kusznir and Park, 1986; Sonder and England, 1986; Meissner and Kusznir, 1987]. From the crustal thickness and composition of island arcs, the rheology might be expected to be intermediate between oceanic and orogenic continental lithosphere as defined by Turcotte [1987]. However, the heat flow across island arcs can be

extremely variable depending on the age of subduction [Hasebe *et al.*, 1970; Anderson *et al.*, 1977; Van den Beukel and Wortel, 1988], making such an interpolation infeasible. Therefore the average rheology of the lithosphere (specifically the effective power law exponent (n)) is kept as an independent variable in our models.

The effective stress-strain exponent (equation (A2)) can vary from $n=1$ for Newtonian fluids to greater values. A value of $n=3$ represents the flow laws for quartz and olivine above the softening temperature and pressure [Goetze and Evans, 1979; Brace and Kohlstedt, 1980] and thus may be similar to the rheology of the

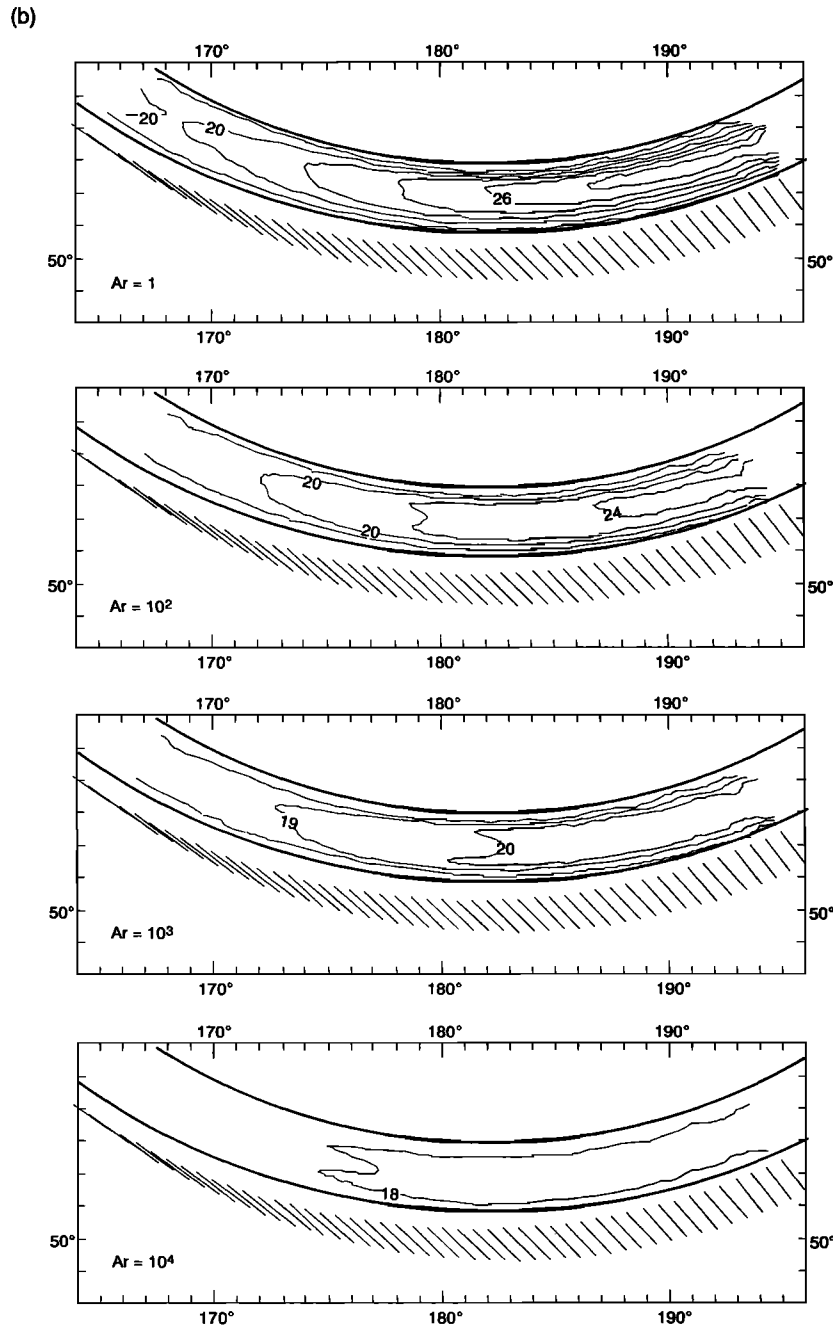


Fig. 6. (continued)

lower crust and mantle. Although n ranges between 2 and 5 for most crustal and mantle rocks [Brace and Kohlstedt, 1980; Kirby, 1983; Kirby and Kronenberg, 1987], larger values of n are tested to explore the effect of plasticity on deformation of the arc lithosphere. High values of n (>10) also imply that friction on faults in the brittle layer is a significant component of the vertically averaged rheology [Sonder and England, 1986]. Our models are similar to those of Fletcher and Hallet [1983] and Bassi and Bonnin [1988a,b], who modeled the brittle upper crust as a continuum and used $n=1000$ to approximate perfect plastic behavior.

The boundary conditions and model geometry are identical to those for the constant velocity gradient model (Figure 2). The thin viscous sheet model also relies on the same assumptions as discussed previously. During the progression of the model over 5

m.y., the width of the deformation zone is fixed at 220 km, implying that new material is added to the arc to compensate for horizontal shortening. Initial thickness of the arc lithosphere and the time-invariant thickness at the Pacific and North American edges are 17 km. Using these boundary conditions, the thin viscous sheet equation is solved in cylindrical coordinates using its finite difference approximation and a cyclic reduction algorithm (Appendix A).

Results

Values for n and Ar were varied independently to observe the effect each parameter has on deformation. Values for α_r and α_θ are constrained so that the small-element rotation along the North American edge approximates the trend defined by rotated

lineaments (Figure 4). For these models, $\alpha_r = \alpha_\theta$ with the values giving the best fit listed in the figure captions. Later, the effects of $\alpha_r \neq \alpha_\theta$ are shown. Other parameters used in the calculations are shown in Table 1. The deformation indicators that are considered below include the stress distribution and crustal thickness.

Figures 5a and 5b shows the principal horizontal deviatoric stresses and crustal thickness, respectively, after 5 m.y. for $n=1, 3, 10,$ and 1000. In addition to the principal stress directions shown in Figure 5a, regions of similar faulting styles in the brittle layer are indicated. These regions are derived from the strain rate tensor as described by *Houseman and England* [1986]. The mnemonics (ST, TS, etc.) represent the two possible styles of faulting (S, strike-slip; T, thrust; N, normal) with the first letter indicating the larger magnitude of the two (see also *Bird* [1989]). Compressive stress is greatest in the eastern part of the arc (region TS) where near-normal convergence occurs. In the far western part of the arc, the two principal stress axes are similar and correspond to a larger component of right-lateral strike-slip faulting (region ST). Little change occurs in the orientation of stresses or style of faulting by increasing n , although increasing n increases the overall magnitude of stress to values that become unrealistic [*Froidevaux et al.*, 1988]. The region of greatest crustal thickness narrows toward the Pacific edge by increasing n (Figure 5b). As indicated by *Sonder and England* [1986], interpretation of n is complex, although it seems to indicate the relative influence of brittle and ductile rheology on the vertically integrated strength. They note that for a brittle-ductile transition depth of 10 km and a Moho temperature of 500°-750°C the effective stress-strain exponent is less than 10. Outside this range of temperature, the effective stress-strain exponent can be larger than 10 and deformation can be considered perfectly plastic, owing to the behavior of rocks either in the upper mantle or the upper crust.

The differences in the deformation of the arc by varying Ar between 1 and 30 are more subtle than those caused by varying n . The orientation of principal stresses for Ar values of 1, 3, and 30 are almost identical, and the thickness of the crust remains essentially unchanged. The lack of significant changes in deformation for Ar less than 30 relates to the short time span of deformation. By tracking deformation over longer time spans such as 20-40 m.y. as done by *England and McKenzie* [1982] and *Houseman and England* [1986], changes in deformation for Ar less than 30 are evident due to the increased importance of buoyancy forces. Higher values of Ar ($Ar=10^2, 10^3,$ and 10^4) were tested to observe the effects on deviatoric stress and thickness as deformation approaches plane horizontal strain (Figure 6). These models used a linear rheology because the algorithm becomes unstable for the nonlinear and high Ar cases. As Ar increases from 10^2 the orientation of principal stresses near the North American edge is increasingly rotated from the orientation of principal stresses near the Pacific edge (Figure 6a). For $Ar=10^4$ (approximately plane horizontal strain), high shear stresses and right-lateral strike-slip faulting are predicted near the North American edge, with a lower magnitude of left-lateral fault-producing stresses occurring near the Pacific edge. This stress field is associated with a velocity field that reaches a maximum in the center of the arc, rather than at the Pacific edge as in Figure 3a. Left-lateral faulting near the Pacific edge is highly unlikely given the direction of plate motion and suggests that a plane horizontal strain model is inconsistent with arc deformation. As expected, increasing Ar decreases the thickness contrast along the arc (Figure 6b).

The effects of specifying boundary conditions such that $\alpha_r \neq \alpha_\theta$ are now investigated. The motivation for specifying velocity boundary conditions of different orientation than the Pacific plate convergence vectors is from analysis of slip vectors from earthquakes in the main thrust zone by *Ekström and Engdahl* [1989]. They find that the slip vectors are oriented closer to arc normal than the plate convergence vectors, suggesting that a portion of the transcurrent slip is accounted for in the overriding plate. Their model of slip partitioning is similar to a model first proposed by *Fitch* [1972], based on the assumption that horizontal shear is more likely to occur on a vertical fault in the overriding plate than the inclined surface of the main thrust zone. Furthermore, this implies that arc-parallel coupling is greater than downdip or arc-normal coupling, presumably owing to bathymetric features aligned sub-normal to the arc [*Ekström and Engdahl*, 1989]. We modify this concept by considering that transcurrent motion transferred to the overriding plate is distributed across the width of the arc rather than along a single fault coincident with the volcanic line [*Fitch*, 1972]. The value for α_r is fixed at 5%, and α_θ is chosen so that the small element rotation best fits the rotated lineaments as before. For $Ar=1$ and $n=1$, the optimal value for α_θ is 35%. This value is less than the value of 60% determined by *Ekström and Engdahl* [1989], but the difference may relate to having the transcurrent motion distributed across the arc. Figure 7 shows the stress field and crustal thickness for this model. Generally, the magnitude of stress is higher to the west in this model, which contrasts with the model shown in Figure 5 ($n=1, Ar=1, \alpha_r=\alpha_\theta=0.30$) where the region of highest stress is in the east. A region of right-lateral strike-slip faulting with secondary normal faulting (SN) is present in the eastern two-thirds of the model (Figure 7a) that is not present in any of the previous models. Also in contrast to previous models, the greatest crustal thickness occurs at the western end of the arc. Higher values of n narrow the crustal ridge toward the Pacific edge, and higher values of Ar decrease the thickness contrast as before.

In summary, increasing Ar tends to shift deformation from being dominantly in a vertical plane to a horizontal plane. The fact that strike-slip faulting is more evident with high Ar is linked to the inability the crust has to sustain thickness contrasts (i.e., thrust faulting [*Houseman and England*, 1986]). Increasing n increases the dominance of brittle or plastic rheology and concentrates deformation near the active boundary (the Pacific edge). It is noteworthy that the thin viscous sheet models show how compressional stresses can dramatically change away from the subduction zone. Only in restricted regions is thrust faulting parallel to both principal stress axes (region TT) present; the majority of the arc has some component of strike-slip faulting, even in regions of near-normal convergence.

6. DISCUSSION

In evaluating the continuum models, we must assume that observations of the upper crust indicate flow for the entire lithosphere. If the average rheology of the lithosphere is close to that of the upper crust, this assumption is valid. For rheology closer to that of the lower crust, this assumption implies that the upper crust must act as a passive indicator of the flow in its substrate. The data we have available to evaluate the models include bathymetry, paleo-declination data, amounts of block rotation, and earthquake focal mechanisms.

The crustal thickness results obtained for the thin viscous sheet models are difficult to evaluate owing to the high amount of

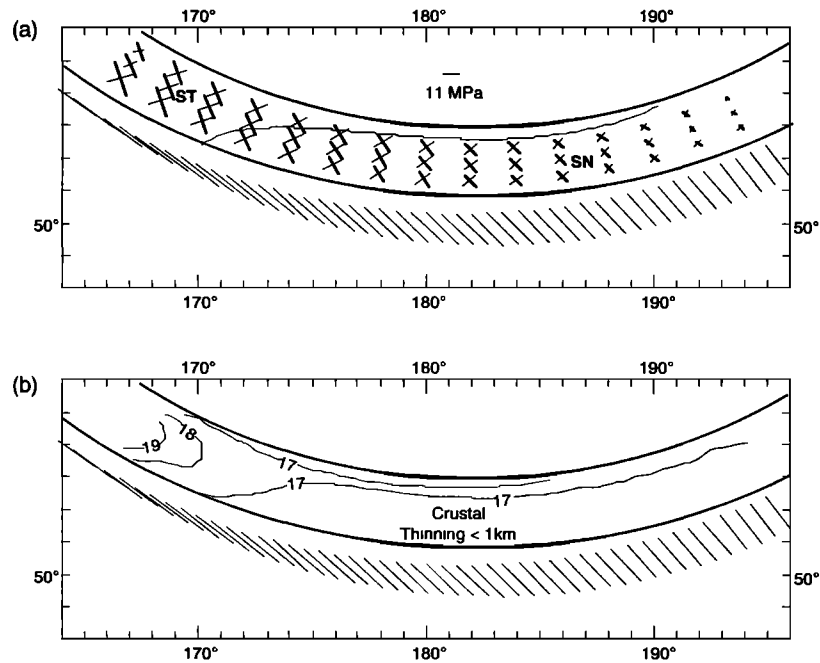


Fig. 7. (a) Principal horizontal deviatoric stresses and (b) crustal thickness for the thin viscous sheet model after 5 m.y. for $Ar=1$, $n=1$, and partitioned boundary conditions: $\alpha_r = 0.05$, $\alpha_\theta = 0.35$. Thin solid line in Figure 7a delineates regions of similar faulting styles [Houseman and England, 1986]. Note that the region of strike slip with secondary normal faulting (SN) is present only for this model. The value for α_θ was chosen to produce the best fit to the rotated lineaments as in Figure 4. Contour interval for crustal thickness diagrams is 1 km. Pacific plate velocity vectors are shown south of the Pacific edge of the arc.

volcanism and presumably related plutonism during the past 5 m.y. The 25 km maximum crustal thickness estimate of Shor [1964] and Grow [1973] in the Adak-Amlia region and the 20-30 km crustal thickness estimate of Gaynanov *et al.* [1968] across the Komandorsky Islands are at least partially attributed to intrusion of subduction-related magmas [Kay and Kay, 1985]. Nonetheless, the more or less constant width and elevation of the arc platform (an erosion surface) seems to rule out any models calling for large along-arc gradients in crustal thickness. Thin viscous sheet models with low values of Ar unrealistically predict locally thickened crust greater than 11 km over the initial thickness and an 8 km gradient in thickness along the length of the arc. The thin viscous sheet models with high values of Ar ($>10^2$) and those with partitioned boundary conditions conform more closely to the lack of large along-arc bathymetric gradients.

Paleomagnetic data [Harbert, 1987] document a clockwise rotation of upper crustal blocks in the Aleutian arc, a motion consistent with the results of most of the models. However, the paleomagnetic data are from Oligocene and Eocene rocks, preventing a quantitative comparison to rotation during the past 5 m.y. described by the models. As previously discussed, lineaments rotated during the past 5 m.y. are used to constrain values for α_r and α_θ .

The stress field within the deformation zone deduced from earthquake focal mechanisms provides important data for evaluating the different models. Right-lateral strike-slip earthquake focal mechanisms are observed along the length of the arc near the North American edge (G. Ekström, personal communication, 1989) but seem to be concentrated at the extreme western part of the arc near the Komandorsky and Near Islands [Newberry, 1983; Cormier, 1975] and near Adak Island [LaForge and Engdahl, 1979; Ekström and Engdahl, 1989]. The concentration of seismicity near Adak Island is most likely influenced by the greater density of seismic stations in the Adak

region. The relative abundance of arc-parallel lineaments to the west [Seliverstov, 1987], presumably from right-lateral shearing, seems to favor high values of Ar ($>10^2$) where large shear stresses are concentrated along the North American edge (Figure 6a). The stress field using partitioned boundary conditions (Figure 7a) is optimal in that it also predicts a component of normal faulting (SN) that agrees with the numerous transverse normal faults present in the eastern two-thirds of the arc. Tensional stresses in the arc massif can also develop simply because of crustal thickness inhomogeneities associated with convergent margins [Artyushkov, 1973; Sleep, 1975; Dalmayrac and Molnar, 1981; Froidevaux *et al.*, 1988]. However, these stresses are directed normal to the arc while normal faulting associated with transverse canyons is associated with arc-parallel tensional stresses.

7. CONCLUSIONS

Continuum models provide a viable method for describing deformation along the Aleutian Island Arc. Simple models, such as those constrained only by having constant velocity gradients, can predict the along-arc trend in small-element rotation but produce unrealistic rates of crustal thickening. In most cases, varying the parameters of thin viscous sheet models produces unique deformation of the arc in terms of the velocity field, deviatoric stress, crustal thickness, and small-element rotation. Based on these observations, thin viscous sheet models, where more arc-parallel motion than arc-normal motion is transferred to the island arc, best describe deformation of the Aleutian Island Arc. These models, modified from those proposed by Fitch [1972] and Ekström and Engdahl [1989] where normal and transcurrent slip is partitioned between the main thrust zone and the overriding plate, respectively, predict a broad region of strike-slip and normal faulting (SN) that geographically corresponds with the region of block rotation and arc-parallel extension of the

arc massif. This model is also consistent with small crustal thickness gradients along the arc. Varying the effective stress-strain exponent does not produce significant enough changes in principal stress orientation or crustal thickness to constrain its value, although $n > 3$ produces unrealistic stress magnitudes.

Viewed from another perspective, the fact that partitioned boundary conditions are optimal in describing the deformation indicates that the normal stress transferred to the arc (σ_{rr}) is small in comparison to the along-arc shear stress ($\sigma_{r\theta}$). Other investigators [von Huene, 1984; Davis and von Huene, 1987; Ryan and Scholl, 1989] have also noted that compressional stress does not seem to be transmitted to the arc massif, at least at shallow levels of the crust. Shear stress in the downdip direction along the main thrust zone is not modelled here and is likely to influence vertical deformation in the outer forearc region.

The models presented here describe a simple homogeneous medium. Several assumptions have been made to cast the geometry of the deforming arc in the horizontal plane so that along-arc variations in boundary conditions can be included. Other models that are more useful in describing forearc and trench dynamics are formulated in the vertical plane to investigate the response of the overriding plate to subduction [e.g., Sleep, 1975; Melosh and Raefsky, 1980; Davies, 1981; Tharp, 1985; Zhang et al., 1985; Sato and Matsu'ura, 1988] and to frictional corner flow below the arc lithosphere [e.g., Sleep, 1975; Tovish et al., 1978; Wdowinski et al., 1989]. Inevitably, the dip of the downgoing plate, the along-strike variability of the convergence vector, and a nonlinear rheology will have to be reconciled in a three-dimensional model. Accounting for the heterogeneity of island arc crust and the thermal structure of the arc would further improve continuum models of island arc deformation.

APPENDIX A

From Cauchy's equations of motion (neglecting the inertia term),

$$\nabla \cdot \sigma = \rho g a \quad (A1)$$

where σ is the stress tensor, $g a$ is the gravitational acceleration vector, and ρ is the density. To find a solution to equation (A1), England and McKenzie [1982] use vertical average of stress and rheology throughout the lithosphere and a power law constitutive relation:

$$\tau_{ij} = B \dot{\epsilon}_{ij}^{(1/n-1)} \dot{\epsilon}_{ij} \quad (A2)$$

where τ is the vertically averaged deviatoric stress tensor defined by

$$\tau_{ij} = \sigma_{ij} + \delta_{ij} p$$

B and n are constants; $\dot{\epsilon}$ is the strain rate tensor; and \dot{E} is given by

$$\dot{E} = (\dot{\epsilon}_{ij} \dot{\epsilon}_{ij})^{1/2}$$

The constant B includes the temperature dependence of rheology. Providing that the variations in crustal thickness are not too large, the thin viscous sheet equation is

$$\nabla^2 \bar{u} = -3\nabla(\nabla \cdot \bar{u}) + 2(1 - \frac{1}{n}) \dot{E}^{-1} [\nabla \dot{E} \cdot \dot{\epsilon} + (\nabla \cdot \bar{u}) \nabla \dot{E}] + 2Ar \dot{E}^{(1/n-1)} s \nabla s \quad (A3)$$

where \bar{u} is the vertically averaged horizontal velocity vector and s is the crustal thickness. Ar in equation (A3) is the Argand number defined in equation (3). In equation (A3), only horizontal spatial derivatives are considered, and the following nondimensionalized parameters are used:

$$(r', s') = (r, s)/L, \quad \mathbf{u}' = \mathbf{u}/u_0, \quad \text{and} \quad t' = tL/u_0$$

(The primes have been dropped in equation (A3).)

The finite difference equivalent of the thin viscous sheet equation (B3) is made using the following approximations:

$$\frac{\partial u}{\partial r} \approx \frac{u_{i,j+1} - u_{i,j-1}}{2\Delta r} = \delta_r u$$

$$\frac{\partial^2 u}{\partial r^2} \approx \frac{u_{i,j+1} - 2u_{i,j} + u_{i,j-1}}{2\Delta r^2} = \delta_r^2 u$$

$$\frac{\partial^2 u}{\partial r \partial \theta} \approx \frac{u_{i+1,j+1} + u_{i-1,j-1} - u_{i+1,j-1} - u_{i-1,j+1}}{4\Delta r \Delta \theta} = \delta_{r\theta}^2 u$$

where Δr and $\Delta \theta$ are the distances between nodes in the finite difference mesh. A similar form is used for derivatives with respect to θ and derivatives of v . For all calculations, a 16 by 16 mesh is used.

The method used to solve the thin viscous sheet equation is similar to that described by England and McKenzie [1982]. The thin viscous sheet equation is reorganized to a Poisson-like form:

$$4r^2 \delta_r^2 u + \delta_\theta^2 u - 4u = 5\delta_\theta v - 4r\delta_r u - 3r\delta_{r\theta}^2 v$$

$$+ 2(1 - \frac{1}{n}) \dot{E}^{-1} \left[\delta_r \dot{E} \dot{\epsilon}_{11} + \frac{1}{r} \delta_\theta \dot{E} \dot{\epsilon}_{12} + \frac{1}{r} \delta_r \dot{E} (\delta_r (ru) + \delta_\theta v) \right]$$

$$r^2 \delta_r^2 v + 4\delta_\theta^2 v - u = 5\delta_\theta u - r\delta_r v - 3r\delta_{r\theta}^2 u + \quad (A4)$$

$$+ 2(1 - \frac{1}{n}) \dot{E}^{-1} \left[\delta_r \dot{E} \dot{\epsilon}_{12} + \frac{1}{r} \delta_\theta \dot{E} \dot{\epsilon}_{22} + \frac{1}{r^2} \delta_r \dot{E} (\delta_r (ru) + \delta_\theta v) \right]$$

where the right-hand side of each equation is made constant by assuming values for u and v . (Initially, u and v are 0 inside the mesh.) New values for u and v are then obtained using a modified version of the Buneman cyclic reduction algorithm [Buneman, 1969] and a cylindrical transformation described by Buzbee et al. [1970]. The new values obtained from the cyclic reduction algorithm are then used to obtain a new constant for the right-hand sides of equation (A4). This process is repeated until the solution for u and v converges to within a specified percentage (1% for these models) over the entire mesh. Figure A1 shows how the solutions converge for two models ($n=3$ and $n=1000$) using the real-time precision indicator (Π') of Bird [1989]:

$$\Pi' = \frac{\text{RMS}(|u|_i - |u|_{i-1})}{\text{RMS}(|u|_i)}$$

where i is the iteration number. Note the increased number of

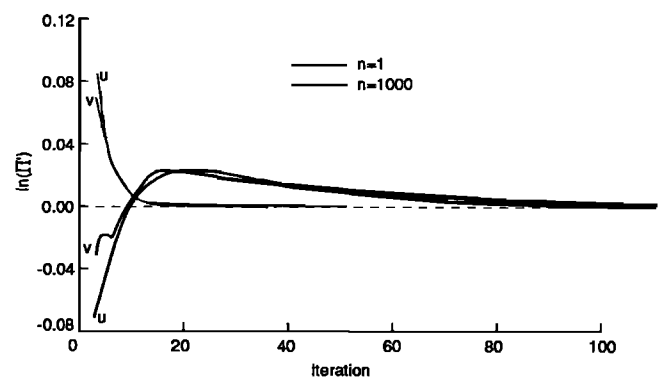


Fig. A1. Convergence of the solution for two models: $Ar=1$, $n=1$ (light lines) and $Ar=1$, $n=1000$ (heavy lines). Iteration number is plotted against the natural logarithm of the real time precision indicator (Π' , see text and Bird [1989] for explanation).

iterations for convergence when $n=1000$. Instability occurs for models with large values of both n and Ar and for α_θ , $\alpha_r > 50\%$, owing to large variations in crustal thickness.

From the velocity values obtained from the thin viscous sheet equation, the time dependence of crustal thickness is determined from the following expression [England and McKenzie, 1982]:

$$\frac{\partial s}{\partial t} = -\nabla \cdot (s\bar{v}) \quad (\text{A5})$$

The value for s is determined by an upwind differencing scheme described by England and McKenzie [1982]. Velocity components are redetermined for each time step using the new crustal thickness values. The deviatoric stress tensor is calculated from equation (A2) with the constant B derived from the definition of Ar in equation (3).

APPENDIX B

The accuracy of the thin sheet assumption with respect to island arcs is tested by calculating the vertical gradient of horizontal stress from the solution to the thin viscous sheet equation (A3). Equation (A1) in cylindrical coordinates is

$$\begin{aligned} \frac{\partial \sigma_{rr}}{\partial r} + \frac{1}{r} \frac{\partial \sigma_{\theta r}}{\partial \theta} + \frac{\partial \sigma_{zr}}{\partial z} + \frac{1}{r} (\sigma_{rr} - \sigma_{\theta\theta}) &= 0 \\ \frac{\partial \sigma_{r\theta}}{\partial r} + \frac{1}{r} \frac{\partial \sigma_{\theta\theta}}{\partial \theta} + \frac{\partial \sigma_{z\theta}}{\partial z} + \frac{1}{r} (\sigma_{r\theta} + \sigma_{\theta r}) &= 0 \\ \frac{\partial \sigma_{rz}}{\partial r} + \frac{1}{r} \frac{\partial \sigma_{\theta z}}{\partial \theta} + \frac{\partial \sigma_{zz}}{\partial z} + \frac{1}{r} \sigma_{rz} &= \rho g a_z \end{aligned} \quad (\text{B1})$$

The thin viscous sheet assumption requires, in part, that

$$\frac{\partial \sigma_{zr}}{\partial z} = \frac{\partial \sigma_{z\theta}}{\partial z} = 0 \quad (\text{B2})$$

Therefore, one measure of error is the residual of the left-hand side of the r and θ equations in (B1) after the value for σ has been calculated using the thin viscous sheet equation. That is, the root-mean-square error can be defined as

$$\varepsilon^2 = \frac{1}{N} \left(\sum \left(\frac{\partial \sigma_{zr}}{\partial z} \right)^2 + \sum \left(\frac{\partial \sigma_{z\theta}}{\partial z} \right)^2 \right) \quad (\text{B3})$$

where N is the total number of nodes in the model. Figure B1 shows how the error varies with the width of the arc ($r_1 - r_0$) for

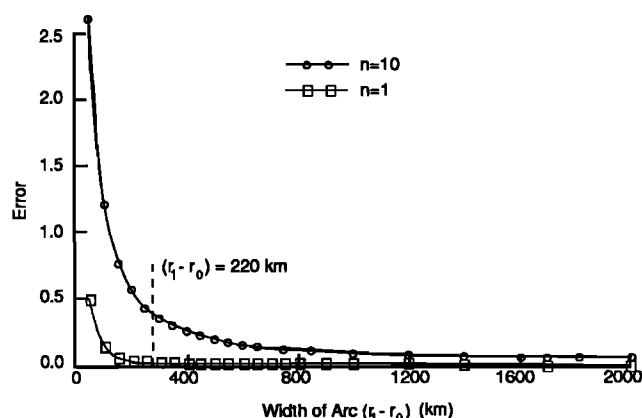


Fig. B1. Accuracy of thin viscous sheet model as a function of the width of the deforming zone for $n=1$ and $n=10$. See text for explanation of how error is measured. Error dramatically increases for narrow deformation zones. Error also increases for all values of ($r_1 - r_0$) as n increases. The width of the deformation zone used for this study (220 km) is shown.

$n=1$ and for $n=10$, holding r_0 constant. As the width of the arc becomes large with respect to the thickness of the lithosphere, the error approaches zero. The error increases abruptly for values of $(r_1 - r_0)/L \leq 3$, the accuracy limit indicated by Artyushkov [1973] for a linear rheology. For nonlinear rheologies, the error increases for all values of ($r_1 - r_0$) as n increases, although not as drastically as decreasing the width of the arc to values less than $3L$.

Acknowledgments. We are grateful to Robert Simpson, Norman Sleep, Andrea Donnellan, an anonymous reviewer, and associate editor David McTigue for insightful and thorough reviews. We also thank Anne Rosenthal for editing the manuscript.

REFERENCES

- Anderson, R. E., Tectonic setting of Amchitka Island, Alaska, *U.S. Geol. Surv. Open File Rep.*, 474-75, rev. 1, 46 pp., 1971.
- Anderson, R. N., S. E. DeLong, and W. M. Schwarz, Thermal model for subduction with dehydration in the downgoing slab, *J. Geol.*, 86, 731-739, 1977.
- Artyushkov, E. V., Stresses in the lithosphere caused by crustal thickness inhomogeneities, *J. Geophys. Res.*, 78, 7675-7708, 1973.
- Bassi, G., and J. Bonnin, Rheological modeling and deformation instability of the lithosphere under extension, *Geophys. J.*, 93, 485-504, 1988a.
- Bassi, G., and J. Bonnin, Rheological modeling and deformation instability of the lithosphere under extension, II, Depth-dependent rheology, *Geophys. J.*, 94, 559-565, 1988b.
- Bird, P., Stress and temperature in subduction shear zones: Tonga and Mariana, *Geophys. J. R. Astron. Soc.*, 55, 411-434, 1978.
- Bird, P., New finite element techniques for modeling deformation histories of continents with stratified temperature-dependent rheology, *J. Geophys. Res.*, 94, 3967-3990, 1989.
- Bird, P., and J. Baumgardner, Fault friction, regional stress, and crust-mantle coupling in southern California from finite element models, *J. Geophys. Res.*, 89, 1932-1944, 1984.
- Bird, P., and K. Piper, Plane-stress finite-element models of tectonic flow in southern California, *Phys. Earth Planet. Inter.*, 21, 158-175, 1980.
- Brace, W. F., and D. L. Kohlstedt, Limits on lithospheric stress imposed by laboratory experiments, *J. Geophys. Res.*, 85, 6248-6252, 1980.
- Buneman, O., A compact non-iterative Poisson solver, *Rep. 294*, 14 pp., Stanford Univ., Inst. for Plasma Res., Stanford, Calif., 1969.
- Buzbee, B. L., G. H. Golub, and C. W. Nielson, On direct methods for solving Poisson's equations, *Siam J. Numer. Anal.*, 7, 627-656, 1970.
- Cooper, A. K., D. W. Scholl, and M. S. Marlow, Plate tectonic model for the evolution of the Bering Sea Basin, *Geol. Soc. Am. Bull.*, 87, 1916-1934, 1976.
- Cormier, V. F., Tectonics near the junction of the Aleutian and Kuril-Kamchatka Arcs and a mechanism for middle Tertiary magmatism in the Kamchatka Basin, *Geol. Soc. Am. Bull.*, 86, 443-453, 1975.
- Cox, A., Rotation of microplates in western North America, in *The Continental Crust and Its Mineral Deposits*, edited by D. W. Strangway, *Spec. Pap. Geol. Assoc. Can.*, 20, 305-321, 1980.
- Dalmayrac, B., and P. Molnar, Parallel thrust and normal faulting in Peru and constraints on the state of stress, *Earth Planet. Sci. Lett.*, 55, 473-481, 1981.
- Davies, G. F., Regional compensation of subducted lithosphere: Effects on geoid, gravity and topography from a preliminary model, *Earth Planet. Sci. Lett.*, 54, 431-441, 1981.
- Davis, D. M., and R. von Huene, Inferences on sediment strength and fault friction from structures at the Aleutian Trench, *Geology*, 15, 517-522, 1987.
- Duncan, R. A., and D. A. Clague, Pacific plate motion recorded by linear volcanic chains, in *The Ocean Basins and Margins*, edited by A. E. M. Nairn, F. G. Stehli, and S. Uyeda, pp. 89-121, Plenum, New York, 1985.
- Ekström, G., and E. R. Engdahl, Earthquake source parameters and stress distribution in the Adak Island region of the central Aleutian Islands, Alaska, *J. Geophys. Res.*, 94, 15,499-15,519, 1989.
- Engelbreton, D. C., A. Cox, and R. Gordon, Relative motions between oceanic and continental plates in the Pacific Basin, *Geol. Soc. Am. Spec. Pap.*, 206, 1986.
- England, P. C., Constraints on extension of continental lithosphere, *J. Geophys. Res.*, 88, 1145-1152, 1983.
- England, P. C., and G. A. Houseman, Finite strain calculations of

- continental deformation, 2, Comparison with the India-Asia collision zone, *J. Geophys. Res.*, **91**, 3664-3676, 1986.
- England, P. C., and D. P. McKenzie, A thin viscous sheet model for continental deformation, *Geophys. J. R. Astron. Soc.*, **70**, 295-321, 1982.
- England, P. C., and D. P. McKenzie, Correction to: A thin viscous sheet model for continental deformation, *Geophys. J. R. Astron. Soc.*, **73**, 523-532, 1983.
- England, P. C., and R. E. Wells, Neogene rotations and quasi-continuous deformation of the Pacific Northwest continental margin, *Geology*, **19**, 978-981, 1991.
- Fitch, T. J., Plate convergence, transcurrent faults, and internal deformation adjacent to southeast Asia and the western Pacific, *J. Geophys. Res.*, **77**, 4432-4460, 1972.
- Fletcher, R. C., and B. Hallet, Unstable extension of the lithosphere: A mechanical model for Basin-and-Range structure, *J. Geophys. Res.*, **88**, 7457-7466, 1983.
- Froidevaux, C. S. Uyeda, and M. Uyeshima, Island arc tectonics, *Tectonophysics*, **148**, 1-9, 1988.
- Gates, O., and W. Gibson, Interpretation of the configuration of the Aleutian Ridge, *Geol. Soc. Am. Bull.*, **67**, 127-146, 1956.
- Gaynanov, A. G., I. P. Kosminskaya, and P. A. Stroyev, Geophysical studies of the deep structure of the Bering Sea, *Izv. Earth Phys.*, no. 8, 3-11, 1968.
- Geist, E. L., J. R. Childs, and D. W. Scholl, The origin of summit basins of the Aleutian Ridge: Implications for block rotation of an arc massif, *Tectonics*, **7**, 327-341, 1988.
- Ghose, R., S. Yoshioka, and K. Oike, Three-dimensional numerical simulation of the subduction dynamics in the Sunda arc region, Southeast Asia, *Tectonophysics*, **181**, 223-255, 1990.
- Gibson, W., and H. Nichols, Configuration of the Aleutian Ridge Rat Islands-Semisopchnoi Island west of Buldir Island, *Geol. Soc. Am. Bull.*, **64**, 1173-1186, 1953.
- Goetze, C., and B. Evans, Stress and temperature in the bending lithosphere as constrained by experimental rock mechanics, *Geophys. J. R. Astron. Soc.*, **59**, 463-478, 1979.
- Grow, J. A., Crustal and upper mantle structure of the central Aleutian Arc, *Geol. Soc. Am. Bull.*, **84**, 2169-2192, 1973.
- Harbert, W. P., New paleomagnetic data from the Aleutian Islands: Implications for terrane migration and deposition of the Zodiac fan, *Tectonics*, **6**, 585-602, 1987.
- Harbert, W. P., D. W. Scholl, T. L. Vallier, A. J. Stevenson, and D. M. Mann, Major evolutionary phases of a forearc basin of the Aleutian terrace: Relation to North Pacific tectonic events and the formation of the Aleutian subduction complex, *Geology*, **14**, 757-761, 1986.
- Hasebe, K., N. Fujii, and S. Uyeda, Thermal processes under island arcs, *Tectonophysics*, **10**, 335-355, 1970.
- Hashimoto, M., Finite element modeling of deformations of the lithosphere at an arc-arc junction: the Hokkaido corner, Japan, *J. Phys. Earth*, **32**, 373-398, 1984.
- Hashimoto, M., Finite element modeling of the three-dimensional tectonic flow and stress field beneath the Kyushu Island, Japan, *J. Phys. Earth*, **33**, 191-226, 1985.
- Houseman, G. A., and P. C. England, Finite strain calculations of continental deformation 1. Method and general results for convergent zones, *J. Geophys. Res.*, **91**, 3651-3663, 1986.
- Kay, S. M., and R. W. Kay, Role of crystal cumulates and the oceanic crust in the formation of the lower crust of the Aleutian Arc, *Geology*, **13**, 461-464, 1985.
- Kirby, S. H., Rheology of the lithosphere, *Rev. Geophys.*, **21**, 1458-1487, 1983.
- Kirby, S. H., and A. K. Kronenberg, Rheology of the lithosphere: Selected topics, *Rev. Geophys.*, **25**, 1219-1244, 1987.
- Kusznir, N. J., and R.G. Park, Continental lithosphere strength: the critical role of lower crustal deformation, in *The Nature of Lower Continental Crust*, edited by J.B. Dawson, D.A. Carswell, J. Hall, and K.H. Wedepohl, *Geol. Soc. Spec. Publ. London*, **24**, 79-93, 1986.
- LaForge, R., and E. R. Engdahl, Tectonic implications of seismicity in the Adak Canyon region, central Aleutians, *Bull. Seismol. Soc. Am.*, **69**, 1515-1532, 1979.
- Marlow, M. S., and A. K. Cooper, Wandering terranes in southern Alaska: The Aleutia microplate and implications for the Bering Sea, *J. Geophys. Res.*, **88**, 3439-3446, 1983.
- Marlow, M. S., D. W. Scholl, E. C. Buffington, and T. R. Alpha, Tectonic history of the central Aleutian Arc, *Geol. Soc. Am. Bull.*, **84**, 1555-1574, 1973.
- McCarthy, J., and D. W. Scholl, Mechanisms of subduction accretion along the central Aleutian Trench, *Geol. Soc. Am. Bull.*, **96**, 691-701, 1985.
- McCarthy, J., A. J. Stevenson, D. W. Scholl, and T. L. Vallier, Speculations of the petroleum geology of the accretionary body: An example from the central Aleutians, *Mar. Pet. Geol.*, **1**, 151-167, 1984.
- McKenzie, D. P., and J. A. Jackson, The relationship between strain rates, crustal thickening, paleomagnetism, finite strain and fault movements within a deforming zone, *Earth Planet. Sci. Lett.*, **65**, 182-202, 1983.
- Meissner, R., and N. J. Kusznir, Crustal viscosity and the reflectivity of the lower crust, *Ann. Geophys.*, **5B(4)** 365-374, 1987.
- Melosh, H. J., and A. Raefsky, The dynamical origin of subduction zone topography, *Geophys. J. R. Astron. Soc.*, **60**, 333-354, 1980.
- Newberry, J. K., Seismicity and tectonics of the far western Aleutian Islands, M. S. thesis, 93 pp., Mich. State Univ., East Lansing, 1983.
- Perry, R. B., and H. Nichols, Bathymetry of Adak Canyon, Aleutian Arc, Alaska, *Geol. Soc. Am. Bull.*, **76**, 365-370, 1965.
- Ryan, H. F., and D. W. Scholl, The evolution of forearc structures along an oblique convergent margin, central Aleutian Arc, *Tectonics*, **8**, 497-516, 1989.
- Sato, T., and M. Matsu'ura, A kinematic model for deformation of the lithosphere at subduction zones, *J. Geophys. Res.*, **93**, 6410-6418, 1988.
- Scholl, D. W., T. L. Vallier, and A. J. Stevenson, Geologic evolution and petroleum geology of the Aleutian Ridge, in *Geology and Resource Potential of the Continental Margin of Western North America and Adjacent Ocean Basins--Beaufort Sea to Baja California*, *Earth Sci. Ser.*, vol. 6, edited by D. W. Scholl, A. Grantz, and J. G. Vedder, pp. 123-155, Circum-Pacific Council for Energy and Mineral Resources, Houston, Tex., 1987.
- Seliverstov, N. I., *Seismo-akusticheskie issledovaniia perekhodnykh zon*, 112 pp., Nauka, Moscow, 1987.
- Shor, G. G., Jr., Structure of the Bering Sea and the Aleutian Ridge, *Mar. Geol.*, **1**, 213-219, 1964.
- Sleep, N. H., Stress and flow beneath island arcs, *Geophys. J. R. Astron. Soc.*, **42**, 827-857, 1975.
- Sonder, L. J., and P. C. England, Vertical averages of rheology of the continental lithosphere: Relation to thin sheet parameters, *Earth Planet. Sci. Lett.*, **77**, 81-90, 1986.
- Sonder, L. J., and P. C. England, Effects of a temperature-dependent rheology on large scale continental extension, *J. Geophys. Res.*, **94**, 7603-7619, 1989.
- Sonder, L. J., P. C. England, and G. A. Houseman, Continuum calculations of continental deformation in transcurrent environments, *J. Geophys. Res.*, **91**, 4797-4810, 1986.
- Spence, W., The Aleutian Arc, tectonic blocks, episodic subduction, strain diffusion, and magma generation, *J. Geophys. Res.*, **82**, 213-230, 1977.
- Tapponnier, P., and P. Molnar, Slip-line field theory and large-scale continental tectonics, *Nature*, **264**, 319-324, 1976.
- Tharp, T. M., Numerical models of subduction and forearc deformation, *Geophys. J. R. Astron. Soc.*, **80**, 419-437, 1985.
- Tovish, A., G. Schubert, and B. P. Luyendyk, Mantle flow pressure and the angle of subduction: Non-newtonian corner flows, *J. Geophys. Res.*, **83**, 5892-5898, 1978.
- Turcotte, D. L., Rheology of the oceanic and continental lithosphere, in *Composition, Structure and Dynamics of the Lithosphere-Asthenosphere System*, *Geodyn. Ser.*, vol. 16, edited by K. Fuchs and C. Froidevaux, pp. 61-67, AGU, Washington, D.C., 1987.
- Vallier, T. L., D. W. Scholl, M. A. Fisher, T. R. Bruns, F. H. Wilson, R. von Huene, and A. J. Stevenson, Geological framework of the Aleutian Arc, in *Geology of North America*, vol. G-1, *Cordilleran Orogen, Alaska*, edited by G. Plafker and D. L. Jones, Geological Society of America, Boulder, Colo., in press, 1991.
- Van den Beukel, J., and R. Wortel, Thermo-mechanical modelling of arc-trench regions, *Tectonophysics*, **154**, 177-193, 1988.
- von Huene, R., Observed strain and the stress gradient across some forearc areas of modern convergent margins, in *Origin and History of Marginal and Inland Seas*, *Proc. Int. Geol. Congr.*, **27th**, **23**, 155-188, 1984.
- Wdowinski, S., and R. J. O'Connell, On the choice of boundary conditions in continuum models of continental deformation, *Geophys. Res. Lett.*, **17**, 2413-2416, 1990.
- Wdowinski, S., R. J. O'Connell, and P. C. England, A continuum model of continental deformation above subduction zones: Application to the Andes and the Aegean, *J. Geophys. Res.*, **94**, 10,331-10,346, 1989.
- Yoshioka, S., The interplate coupling and stress accumulation process of large earthquakes along the Nankai trough, southwest Japan, derived

- from geodetic and seismic data, *Phys. Earth Planet. Inter.*, **66**, 214-243, 1991.
- Yoshioka, S., and M. Hashimoto, A quantitative interpretation on possible correlations between intraplate seismic activity and interplate great earthquakes along the Nankai trough, *Phys. Earth Planet. Inter.*, **58**, 173-191, 1989.
- Yoshioka, S., M. Hashimoto, and L. Hirahara, Displacement fields due to the 1946 Nankaido earthquake in a laterally inhomogeneous structure with the subducting Philippine Sea plate--A three-dimensional finite element approach, *Tectonophysics*, **159**, 121-136, 1989.
- Zhang, J., B. H. Hager, and A. Raefsky, A critical assessment of viscous models of trench topography and corner flow, *Geophys. J. R. Astron. Soc.*, **83**, 451-475, 1985.
-
- E. L. Geist and D. W. Scholl, U.S. Geological Survey, 345 Middlefield Road, MS 999, Menlo Park, CA 94025.

(Received May 16, 1990;
revised November 15, 1991;
accepted December 4, 1991.)